ARCHIVIO ISTITUZIONALE
DELLA RICERCA

Alma Mater Studiorum Università di Bologna
Archivio istituzionale della ricerca

Mechatronic Development of a Climbing Robot for Continuous WAAM 3-D Printing

This is the final peer-reviewed author's accepted manuscript (postprint) of the following publication:

Published Version:
Govoni, A., Arrè, L., Joseph, R., Samorì, D., Ascari, A., Palermo, M., et al. (2026). Mechatronic Development of a Climbing Robot for Continuous WAAM 3-D Printing. IEEE/ASME TRANSACTIONS ON MECHATRONICS, 1, 1-12 [10.1109/TMECH.2026.3695994].

Availability:
This version is available at: https://hdl.handle.net/11585/1075934 since: 2026-08-05

Published:
DOI: http://doi.org/10.1109/TMECH.2026.3695994

Terms of use:

Some rights reserved. The terms and conditions for the reuse of this version of the manuscript are specified in the publishing policy. For all terms of use and more information see the publisher's website.

This item was downloaded from IRIS Università di Bologna (https://cris.unibo.it/).
When citing, please refer to the published version.

(Article begins on next page)

17 November 2026

Mechatronic Development of a Climbing Robot for Continuous WAAM 3D Printing

Journal:	*Transactions on Mechatronics*
Manuscript ID	TMECH-02-2026-23810
Manuscript Type:	Regular paper
Date Submitted by the Author:	07-Feb-2026
Complete List of Authors:	Govoni, Andrea; Universita degli Studi di Bologna Scuola di Ingegneria Arrè, Lidiana; Universita degli Studi di Bologna Scuola di Ingegneria Joseph, Robin; Universita degli Studi di Bologna Scuola di Ingegneria, Dei Samorì, Davide ; Universita degli Studi di Bologna Scuola di Ingegneria Ascari, Alessandro; Universita degli Studi di Bologna Scuola di Ingegneria, DIN Palermo, Michele; Universita degli Studi di Bologna Scuola di Ingegneria Palli, Gianluca (Smart Actuation FS TE); Universita degli Studi di Bologna Scuola di Ingegneria
Keywords:	Manufacturing, Design methodology for mechatronics < Modeling and design, Robotics, Smart building technologies < System integration
Are any of authors IEEE Member?:	Yes
Are any of authors ASME Member?:	No
Note: The following files were submitted by the author for peer review, but cannot be converted to PDF. You must view these files (e.g. movies) online.	
Rebut_medium_qual.mp4	

SCHOLARONE™
Manuscripts

Mechatronic Development of a Climbing Robot for Continuous WAAM 3D Printing

Andrea Govoni[1], Lidiana Arrè[2], Robin Joseph[1], Davide Samorì[1], Alessandro Ascari[3], Michele Palermo[2], Gianluca Palli[1]

***Abstract*—Wire Arc Additive Manufacturing (WAAM) is widely used in industry for high-deposition-rate metal fabrication. However, extending WAAM to large-scale and, in particular, vertical self-supporting structures remains challenging, since process geometric variability compromises reliable referencing, positioning, and autonomous on-structure operation. This paper presents a Climbing Mobile 3D Printer (CM3DP) tailored for continuous WAAM of self-supporting metal structures. Because WAAM produces irregular geometries that make conventional climbing unreliable, the robot integrates motion and deposition in a single frame and uses a discrete, print-embedded guiding and anchoring mechanism to climb robustly. Bayesian Optimization is used online to adapt the climbing strategy and compensate for defects and positioning uncertainties. This integration facilitates the fabrication of large-scale, vertical structures with enhanced flexibility and automation. The paper details the mechatronic design of the CM3DP, the integration of hardware and software components, the structural design of the printed elements, and experimental validation of the climbing and anchoring strategies, and WAAM deposition using CM3DP.**

***Index Terms*—Wire Arc Additive Manufacturing, 3D Printing, Mobile Additive Manufacturing, Robotic Climbing Systems, Continuous 3D Printing for self-supporting Structures, Mechatronic Design for WAAM Robots.**

I. Introduction

Since the early 21st century, automation has made significant strides in industrial sectors such as automotive, aerospace, and biomedical; however, its integration in the construction industry remains relatively underdeveloped. This gap is mainly due to the complexity of custom components and specialized subsystems, which has steered construction automation toward prefabricated assembly and in-situ Additive Manufacturing (AM) [1]. In this context, integrating robotics with AM requires not only additive processes capable of producing durable, high-performance materials [2], but also robotic systems that can operate autonomously in dynamic construction environments.

Among metal AM processes, Wire Arc Additive Manufacturing (WAAM) is a Direct Energy Deposition (DED) approach that employs standard welding equipment (arc welder and wire feedstock) with robotic or CNC-controlled motion to deposit metal layer-by-layer. In steel structures, it is well suited thanks to high deposition rates and efficient material use, and it supports repair-focused designs and hybrid construction workflows [3]–[6]. WAAM structures are typically produced either by continuous layer deposition, commonly adopted for shell-based elements [7]–[9], or by dot-by-dot deposition for strut-based lattice elements [10], [11]. The adoption of WAAM for structural applications has been supported by extensive investigations on the mechanical response, as well as on the microstructural and geometric features of WAAM-produced elements, including process-induced geometrical irregularities such as lack of straightness, surface roughness, and cross-sectional variability [7], [11]–[15]. Overall, these studies show that WAAM materials can exhibit mechanical responses different from their wrought counterparts, and that structural demonstrators have validated the feasibility of fabricating large-scale, complex steel and structures, predominantly via continuous layer deposition. Representative examples include the MX3D steel pedestrian bridge [16], the 3D-printed steel garden bridge [17], the in-situ printed footbridge at TU Darmstadt [18], and strengthening systems for historic masonry using WAAM steel meshes [19].

In parallel, onsite AM platforms have evolved from gantry-based systems [20] to robotic-arm solutions [21] and, more recently, mobile platforms; nevertheless, fabricating complex geometries still faces limitations in scalability and precise process control [22]. For WAAM in particular, while continuous deposition aligns well with Mobile Additive Manufacturing (M-AM) principles [23], process-induced surface irregularities make reliable robotic climbing and anchoring on the printed structure especially challenging.

This work presents a Climbing Mobile 3D Printer (CM3DP) for WAAM-based M-AM (Fig. 1) that overcomes prior onsite mobile printing limits by replacing gear-and-rack locomotion [24] with a discrete guiding and anchoring strategy robust to WAAM-induced geometric variability. Specially shaped indentations (Anchor Points) are embedded in the printed WAAM-produced element to provide robust grasping and reliable climbing despite surface irregularities. To cope with residual uncertainties, the system employs online Bayesian Optimization (BO) to adapt the climbing procedure and ensure consistent clamping.

The paper is organized as follows: Sec.II reports relevant literature, while the design of the self-supported printed structure (called WAAM-produced element) is presented in Sec. III. The mechanical design of the CM3DP is detailed in Sec. IV and its hardware-software framework is described in Sec. V. The optimization of the climbing process is reported in Sec. VI while experimental validation of the climbing mechanism and WAAM deposition is shown in Sec. VII.

[1]A.Govoni, R.Joseph D.Samorì and G.Palli are with the Department of Electrical, Electronic, and Information Engineering (DEI), University of Bologna, Italy.
[2] L.Arrè and M.Palermo are with the Department of Civil, Chemical, Environmental, and Materials Engineering (DICAM), University of Bologna, Italy.
[3] A.Ascari is with the Department of Industrial Engineering (DIN), University of Bologna, Italy.

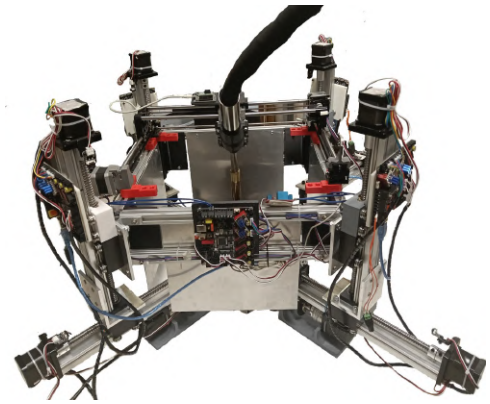

(a) Complete CM3DP, with weld spatter protection barriers.

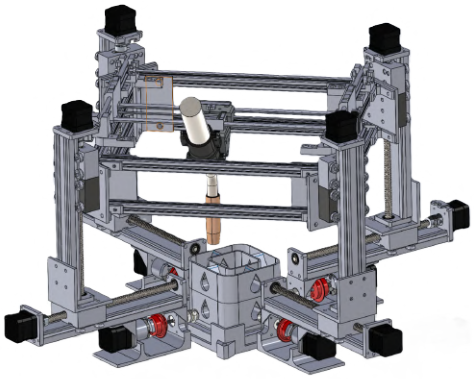

(b) The CM3DP (CAD).

(c) Selco GSM-352Torch Welder.

Fig. 1: CM3DP component highlights.

II. Related Work

Early large-scale 3D printing relied on slow gantry machines and track-mounted rovers whose size was comparable to the printed elements [25]. To gain flexibility, printing systems were mounted on robotic arms, reducing the mechanical footprint to the arm itself while extending the reachable workspace [26]. Even so, reach limitations remained, so multiple arms were adopted to enlarge the effective printing area, enabling bigger parts but not truly removing workspace constraints [27]. More recently, conveyor-belt solutions and mobile manipulator robots have been proposed to further increase printable dimensions, yet they still impose overall dimensional limits [28], [29].

The development of mobile small-scale robots originally designed for inspection and maintenance [30], [31] has expanded the workspace for large-scale 3D printing in construction [32], [30], [33], [34]. In addition to the robot mobility explored in the literature [35], [36], a novel paradigm is emerging: robotic printers that not only fabricate self-supporting structures but also ascend them during the construction process [24], [37]–[40]. For this purpose, several robots have been designed to traverse complex 3D environments while maintaining adhesion against gravity, for instance through modular anchoring points [41] or suction-based climbing systems [39], [42]. However, these adhesion methods depend heavily on the material properties, limiting their adaptability to different printing materials.

In addition, in M-AM, some systems are equipped with gear wheels that engage with racks integrated into the printed structure [37], [40], [24]. These solutions enable continuous climbing along the printed element and rely on advanced clamping mechanisms where gear wheels and integrated racks serve as guiding and anchoring components. Although the existing climbing concepts are effective in their intended settings , their performance degrades in the WAAM context, where deposition inherently produces surface irregularities and local geometric deviations that compromise the repeatable contact and alignment required for guidance and anchoring, ultimately limiting reliable climbing on the printed structure.

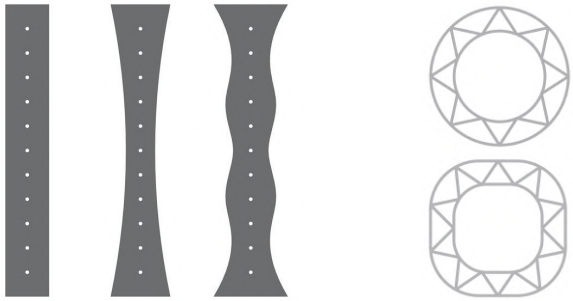

(a) Longitudinal Development. (b) Cross section.

Fig. 2: WAAM-Enabled Applications and Design.

III. WAAM-produced self supporting structure enabled by the CM3DP

The proposed CM3DP system is designed to fabricate self-supporting structures characterized by a predominantly longitudinal development and potentially infinite length. By eliminating the need for external support during fabrication, these structures enable fully autonomous additive erection. Within this framework, the current CM3DP system enables the realization of elements with novel and geometrically complex cross-sectional configurations, as illustrated in Fig. 2b [9], provided that suitable deposition inclinations compatible with WAAM process constraints are adopted. Such elements can therefore be interpreted as individual components or portions of more articulated structural systems. While longitudinal WAAM elements with complex geometrical features have already been explored, the proposed approach advances the state of the art by integrating discrete anchoring holes (Fig. 2a), enabling the printer to grip, move, and incrementally erect self-

TABLE I: Anchor Points's height statistics: first WAAM-produced element and second WAAM-produced element.

Parameters	First Element	Second Element
Nominal height (mm)	35.0	35.0
Maximum height (mm)	36.0	38.0
Minimum height (mm)	33.0	24.5
Average height (mm)	34.5	29.7
Standard deviation (mm)	1.2	4.8

TABLE II: Diameter statistics of Anchor Points: First WAAM-produced element and Second WAAM-produced element.

Parameter	First Element	Second Element
Nominal diameter (mm)	21.0	21.0
Maximum diameter (mm)	21.5	22.0
Minimum diameter (mm)	20.0	20.0
Average diameter (mm)	21.2	21.7
Standard deviation (mm)	0.7	0.8

supporting elements. Nevertheless, the fabrication of elements incorporating such features presents considerable challenges. The deposition of molten metal over hollow or unsupported regions is susceptible to deformation and sagging due to gravity, while the lack of a continuous substrate limits the achievable accuracy of overhanging geometries.

To demonstrate the feasibility of CM3DP to grip and move along the WAAM-produced element, a WAAM basement was fabricated for the CM3DP prototype (Fig. 3). The element consists of inner and outer walls arranged in a square cross-section with rounded corners, with edge lengths of 72 mm and 120 mm, respectively. The wall thickness is 3.2 mm, while the anchoring hole depth is 28 mm (Fig. 3a). These walls extend longitudinally along a straight path and are connected through specially designed anchoring holes, referred to as Anchor Points in Fig.3c, 3d. Each Anchor Point features a drop-shaped geometry, combining a lower circular section with an upper tapered region inclined at 60°. This configuration promotes the gradual bridging of molten metal during deposition, thereby reducing sagging and preserving structural continuity in unsupported regions. The Anchor Points have a height of 35mm and a diameter of 21mm, dimensions optimized to ensure manufacturability and geometric reliability within WAAM constraints (see Fig. 3d). The Anchor Points are symmetrically placed around the basement to ensure compatibility with the CM3DP 's Anti-Pullout System.

In addition to this first configuration, a second basement was fabricated featuring two longitudinal levels of Anchor Points 3b. This solution was introduced to assess how the presence

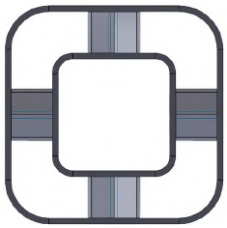

(a) Cross-section.

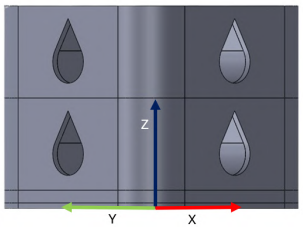

(b) 3D Iso view.

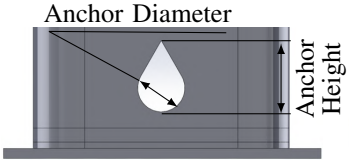

(c) Frontal view highlighting anchor point.

(d) Real WAAM-produced element.

Fig. 3: WAAM-produced basement for the CM3DP prototype.

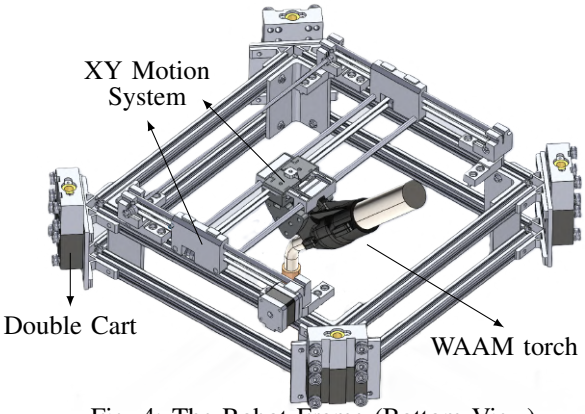

Fig. 4: The Robot Frame (Bottom View).

of multiple anchoring levels influences the repeatability of the Anchor Points geometry within the same WAAM-produced element, and to enable validation of the proposed approach through CM3DP climbing on a two-level basement, thereby demonstrating the feasibility of climbing on elements characterized by an increased number of anchoring levels.

Due to printing irregularities inherent to the WAAM process, the shape and size of the Anchor Points may vary both between different WAAM-produced structures and within a single structure. As shown in Tab.II, the selected solution for manufacturing the Anchor Points exhibits minimal variation across identical basements, indicating good repeatability in line with both the design requirements and the current capabilities of WAAM technology. This analysis was performed by considering both basement configurations previously introduced, in order to evaluate the variability in the shape and dimensions of the Anchor Points when multiple anchoring levels are realized within the same WAAM-produced element. As reported in Tab. I, the Anchor Point Height exhibits higher variability, which is more pronounced in the second configuration when the measurements account for both anchoring levels of the same basement. Nevertheless, the adopted drop-shaped design for the Anchor Points has proven to be effective, as it ensures consistent diameters at the insertion region required for plug insertion. This behaviour can be attributed to gravity-induced deformation occurring predominantly in the upper tapered portion of the Anchor Points, which does not affect the critical diameter. As a result, reliable insertion performance is maintained despite local geometric variations.

IV. CM3DP Mechanical Design

The proposed CM3DP is designed to scale the WAAM-produced element almost infinitely by leveraging WAAM technology and a discrete guiding system embedded within the WAAM-produced element, enabling the fabrication of tubular metal components with predominant longitudinal development, such as beams, columns, truss systems, and lighting poles, as illustrated in Fig. 3b.

A. Robot Frame

Fig. 4 shows the Robot Frame, which consists of two rectangular frames joined by corner coupling plates, forming a rigid

skeletal structure. The Robot Frame supports the X–Y linear motion system, including the X- and Y-axis linear guides. The printing head comprises the welding torch, connected to the Selco GSM-352 (Fig. 1c) power source and the WAAM wire feeder. Planar motion of the WAAM torch is achieved by two stepper motors (one per axis) driving toothed-belt transmissions. The Z-axis is actuated by four Vertical Actuator actuators mounted on the Robot Frame, which move the torch up and down to reach the desired deposition height.

B. Motion Legs

Fig.9 shows a single leg, composed of a Vertical Actuator, a Horizontal Actuator, and a Anti-Pullout System mechanism. When actuated together, the Motion Legs provide the torch motion along the Z axis.

A leg can also be commanded individually to securely grip the Anti-Pullout System mechanism in its dedicated shaped holes in the walls of the WAAM-produced element, enabling the CM3DP to remain firmly attached during both printing and climbing. For Anti-Pullout System insertion of a single leg (e.g. Leg1 in Fig. 9), a tool frame Σ_{tool} is defined at the tip of the Anti-Pullout System and it is driven to arrive at Σ_{target} coordinates expressed in the world frame. Assuming zero relative rotation and expressing the motion in Σ_{tool}, the Vertical Actuator translates Σ_{tool} along Z, the Horizontal Actuator translates along X, and the adjacent Motion Legs (Leg 2 and Leg 3 in Fig. 9) provide the required translation along Y.

As shown in Fig. 6 and Fig. 7, both the Vertical Actuator and Horizontal Actuator actuators are based on NEMA17 stepper motors driving lead screws and a carriage system. This ball-screw architecture was selected to provide a stiff and efficient rotary to linear conversion together with adequate load capacity. Each actuator is rated for a maximum axial force of 200 N; therefore, the four Vertical Actuator actuators provide an overall vertical load capacity of 800 N.

Mechanical end-stops are installed at both stroke extremities to define the zero reference. A flexible coupling, placed under the end-stop, compensates for residual shaft misalignment, while a support bearing improves guidance and reduces bending loads on the screw.

We want to note that the additional 3D-printed carriage on the Vertical Actuator (Fig. 8) provides a second frame anchoring point, increasing leg stiffness and reducing deformation under load. It uses brass inserts, a brass bushing, and bearings to add extra screw attachment points and ensure smooth guidance along the linear guide and lead screw, improving rigidity and anchoring accuracy.

C. Clamping Device

Figure 10a shows the Clamping Device mechanism, integrating a NEMA17 stepper motor with a planetary gearbox, an end stop, and a 3D-printed prismatic coupling (red). The coupling drives a screw inside the Anti-Pullout System: looking at (Fig. 10b), when the screw advances, it forces the locking balls outward to press against the inner wall of the WAAM-fabricated anchoring hole, securing the leg. This clamping action can exert a gripping force of up to 3.3 kN. Since the torque required to tighten the screw (2 Nm) exceeds what the motor alone can provide (0.44 Nm), the system incorporates a 1:5.3 planetary gearbox to amplify torque. When the motor reverses direction, the screw retracts and the balls return to their seats, releasing the clamp.

For clarity, we want to highlight that the tool frame Σ_{tool} of Fig. 9 is defined at the tip of the Anti-Pullout System mechanism of Fig. 10b. The insertion task is this formulated as driving the four Σ_{tool} of the four legs into the desired insertion pose Σ_{target}, corresponding to the anchoring-hole entry point.

V. Control Architecture

This section outlines the hardware and software architecture of the CM3DP control system, organized by functional subgroups: the Robot Frame subgroup and four Climbing Device subgroups, each consisting of one Motion Leg and its associated Clamping Device.

Each subgroup is managed by a BigTreeTech (BTT) SKR v3.0 motherboard (referred to as the Control Board), which

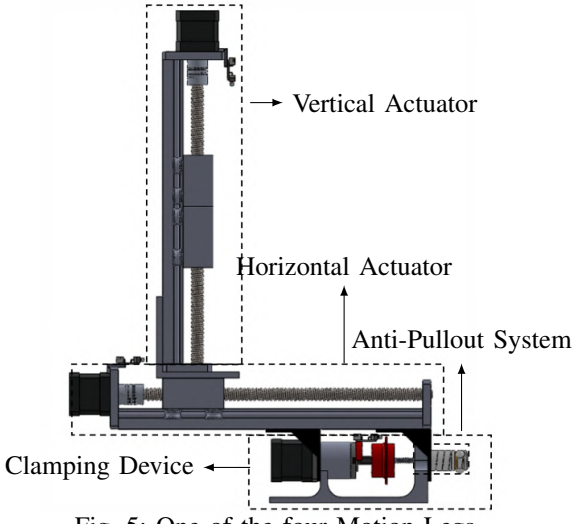

Fig. 5: One of the four Motion Legs.

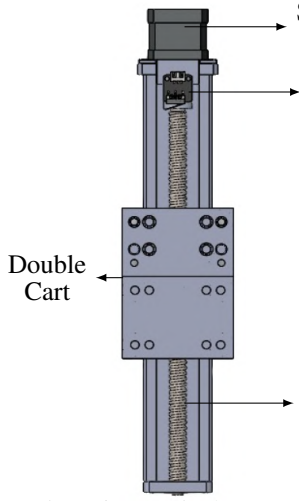

Fig. 6: Vertical Actuator Top View.

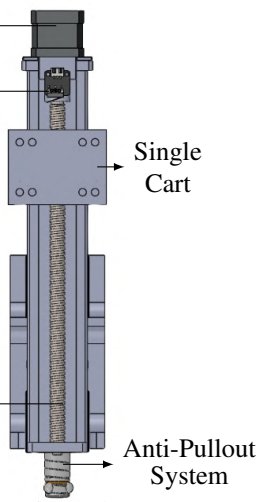

Fig. 7: Horizontal Actuator Top View.

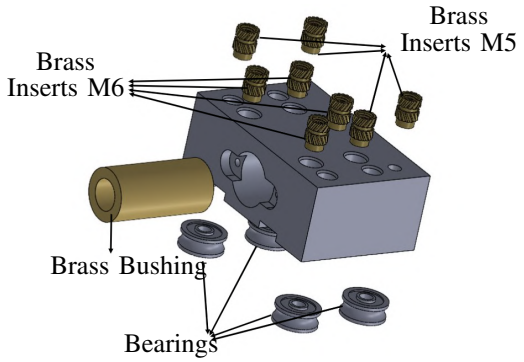

Fig. 8: Second chart Composition.

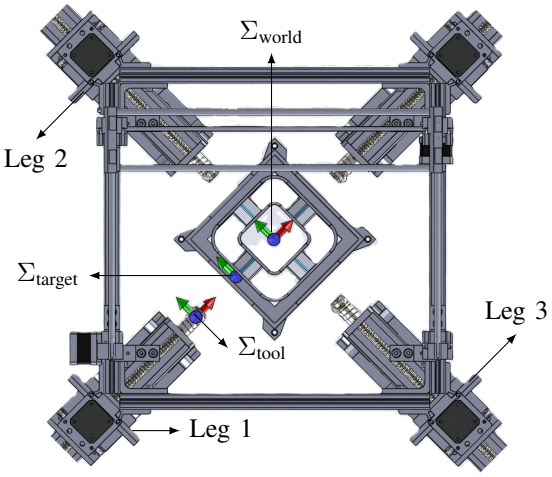

Fig. 9: Frame-Leg Kinematic for Anti-Pullout System insertion Top Overview.

controls the actuators and devices within its group. The SKR v3.0 features a 32-bit ARM Cortex-M7 STM32H743VIT6 processor running at 480 MHz. A relay interfaces the Frame Control Board with the Selco power source and switches the torch on and off. Each Control Board is able to connect via USB with a central PC for system monitoring via serial communication. Designed for 3D printers, the Control Board runs the open-source Marlin firmware [43], which interprets G-code to coordinate multi-axis stepper motion and basic I/O. Commands are transmitted to the Motion Legs and Robot Frame Control Boards via serial communication.

A. Multi-board Marlin control and G-code dispatch

Since the platform comprises five independent motion subsystems, this section describes the pipeline used to parse and dispatch motion commands to the Control Boards for coordinated control of the CM3DP.
Each leg is modeled as a Cartesian robot, therefore, each subsystem is commanded through standard Marlin G-code primitives. As described in Tab. III, we map the three leg actuation modes to the logical axes as follows: Vertical Actuator is assigned to the Marlin Z axis, Horizontal Actuator to the X axis, and Anti-Pullout System to the Y axis. The Robot Frame subsystem is controlled by a dedicated board using a conventional planar mapping, described in Tab. IV. In addition to motion control, this board drives an external relay used to switch the Selco welder torch on and off via a digital output. The host PC acts as the master controller, parsing the standard G-code and routing each motion block to the appropriate Marlin board, thus coordinating all subsystems without requiring board-level awareness of the multi-board architecture.

TABLE III: Basic G-code commands of a single Motion Leg Control Board.

Command	Description
G1 X⟨pos⟩F⟨vel⟩	Linear movement for the Horizontal Actuator
G1 Y⟨pos⟩F⟨vel⟩	Linear movement for the Anti-Pullout System
G1 Z⟨pos⟩F⟨vel⟩	Linear movement for the Vertical Actuator
G28 X Y Z	Homing all three axes or just one if specified
M17 X Y Z	Enables hold torque for one or more steppers
M410	Stop all steppers instantly
M122 S1	TMC debug for stall torque

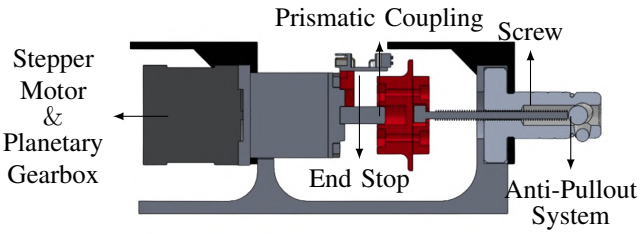

(a) Clamping Device actuator layout.

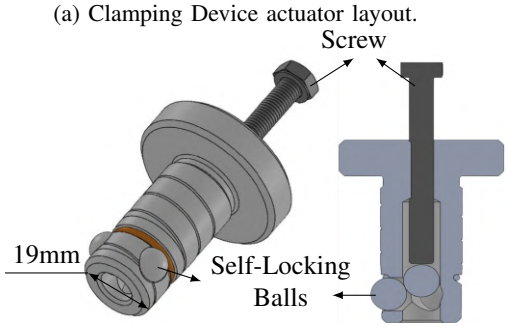

(b) Anti-Pullout System isometric and section view.

Fig. 10: Clamping Device mechanism overview and Anti-Pullout System section details.

B. Stepper Motor Control

The CM3DP employs standard NEMA17 two-phase stepper motors driven by onboard TMC2209 drivers, that enables microstepping to improve smoothness and positional accuracy and sensorless stall detection to provide a measure of interaction forces. For accurate motion control, each leg actuation unit is calibrated to map commanded microsteps to the actual linear displacement of the mechanism. Let N_{steps} denote the motor resolution (e.g., 1.8° per step, i.e., 200 steps/rev) and

TABLE IV: Basic G-code commands of a single Robot Frame Control Board.

Command	Description
G1 X⟨pos⟩ F⟨vel⟩	Linear motion along the Robot Frame X axis
G1 Y⟨pos⟩ F⟨vel⟩	Linear motion along the Robot Frame Y axis
M410	Stop all steppers instantly
G28 X Y	Homing Robot Frame axes or just one if specified
M42 P0 S255	**Torch ON**: set pin HIGH to energize the relay
M42 P0 S0	**Torch OFF**: set pin LOW to de-energize the relay

$N_{\text{microsteps}}$ the microstepping factor (e.g., 16 with the TMC drivers). We define the microstepping resolution as the number of microsteps per millimeter of device motion, denoted as N_{device}, which provides the direct conversion between G-code position commands and physical displacement.

1) Vertical Actuator and Horizontal Actuator: holds

$$N_{\text{LEG}} = \frac{N_{\text{steps}} N_{\text{microsteps}}}{P_{\text{screw}}} \tag{1}$$

where P_{screw} is the pitch of the lead screw used in the transmission.

2) Anti-Pullout System: Consider the configuration shown in Fig. 10, where the lead screw pushes the first sphere along the $x-$axis, this movement resuts in a displacement of the othere spheres out from their headquarters long the y-axis. Let the four spheres of the Anti-Pullout System have radius R and be initially arranged with center-to-center distance $2R$ and angular spacing θ, then it can be proved that a displacement y of the shere outside the clamping system can be given using a screw displacement (x):

$$y(x) = \sqrt{4R^2 - (2R\cos\theta - x)^2} - 2R\sin\theta. \tag{2}$$

Then, the number of microsteps per mm N_{CLAMP} to move the sphere out from Clamping Device.

$$N_{\text{CLAMP}} = x\frac{N_{\text{steps}} N_{\text{microsteps}}}{P_{\text{screw}} n} \tag{3}$$

where n is the the gearbox transmission ratio.

3) Robot Frame: the number of microsteps per mm N_{FRAME} for the Robot Frame motors can be defined as

$$N_{\text{FRAME}} = \frac{N_{\text{steps}} N_{\text{microsteps}}}{2\pi R_{\text{pulley}}} \tag{4}$$

where R_{pulley} is the radius of the transmission pulley.

C. Robot Frame control with IMU

To ensure that the Robot Frame remains balanced and its center of mass stays centered during and at the end of the anchoring phase, we employ the STEVAL-MKI210V2K Inertial Measurement Unit (IMU). The IMU board is placed at the top of the Robot Frame cart, namely above the torch holder.

This IMU integrates accelerometers to measure gravitational forces along different axes, enabling monitoring and control of the Robot Frame 's attitude to detect and correct excessive tilting caused by WAAM Technology uncertainties during the climbing phase. In this way, the Robot Frame subgroup controller can detect the printing plane orientation and eventually command the Motion Legs subgroups to move in order to compensate the misalignment.

Given the accelerometer measurments A_X, A_Y, A_Z and according to rotation representation reported in Fig. 11, the

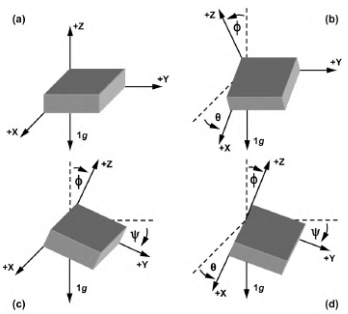

Fig. 11: Frame angular correction: a) and b) show the direction of the detectable acceleration, c) and d) show the direction of detectable angular rate.

Robot Frame tilt angles are calculated using the following equations:

$$\theta = \arctan\left(\frac{A_X}{\sqrt{A_Y^2 + A_Z^2}}\right) \tag{5}$$

$$\psi = \arctan\left(\frac{A_Y}{\sqrt{A_X^2 + A_Z^2}}\right) \tag{6}$$

$$\phi = \arctan\left(\frac{\sqrt{A_X^2 + A_Y^2}}{A_Z}\right) \tag{7}$$

We assume that the X and Y IMU axis are aligned with the frame's corner-to-corner directions (i.e., the lines joining opposite legs) and the IMU is placed at the center of the Robot Frame during the balancing phase. Considering the Robot Frame as a parallelepiped with diagonals l_X and l_Y, see Sec. IV-A, to realign it with the horizontal plane, the two Motion Legs rotating the frame along the X-axis, i.e. the two Motion Legs placed along the Y-Axis, must be moved along the Vertical Actuator by

$$\Delta_{XZ} = \pm\frac{l_Y}{2}\sin(\psi) \tag{8}$$

while the two Motion Legs rotating the frame along the Y-axis (i.e. the two Motion Legs placed along the X-Axis) must be moved along the Z-axis by

$$\Delta_{YZ} = \pm\frac{l_Y}{2}\sin(\theta) \tag{9}$$

The sign of the displacement to be applied to the Motion Legs depends on which side of the Robot Frame the Motion Leg is placed and on the sign of the corresponding rotation generated by the Motion Leg. This formulation lead to a symmetric correction, while a leg rises the other must descend.

VI. Climbing Optimization

During the climbing and anchoring phase, the insertion of the Clamping Device into the Anchor Points presents significant challenges due to WAAM-induced irregularities, such as burrs and geometric deviations. These issues introduce uncertainty in the true position of the Anchor Points complicating the insertion process. To address this problem, BO is exploited, as illustrated in Fig. 12 and detailed in Alg. 1,

Algorithm 1 Clamping Procedure with Bayesian Optimization

if Homing is completed **and** current layer is printed **then**
  for each leg from 1 to 4 **do**
    if the layer is not the first **then**
      Disarm the leg from the hole
    end if
    for $i = 1$ to N **do**
      Get $x0_i$, $y0_i$, $z0_i$ from G-Code
      Lift the vertical actuator to $z0_i$
      Move the horizontal actuator $(x0_i, y0_i)$
      while insertion is in progress **do**
        Continuously monitor f_{motor}
        if load exceeds threshold **then**
          Stop insertion
          Compute Cost J_{BO}
          Update BO with (x_i, y_i, z_i, J_{BO})
          Select next candidate x_i, y_i, z_i using AF
        end if
      end while
      Push the sphere out to secure the clamp if horizontal actuator arrived to position
    end for
  end for
  Check for misalignment using the IMU board
end if

to obtain a robust approach able to simultaneously handle WAAM uncertainties and potential actuator step losses.

BO is particularly suited for this task, as it efficiently handles optimization problems characterized by a limited number of input variables (typically $\leq$20) and unknown objective functions modeled as black boxes [44]. The BO framework relies on a probabilistic model, typically a Gaussian Process (GP), to approximate the objective function over the search space. This model allows the algorithm to leverage information from previous evaluations to guide the selection of new candidate points. An Acquisition Function (AF) selects the next sampling point by balancing exploration of uncertain regions and exploitation of high-performing areas, enabling efficient search by discovering promising new zones while refining known good solutions. So, the algorithm aims to iteratively refine the estimated position of the plug, starting from an initial guess of the Anchor Points location. At each iteration, the AF is implemented using the Expected Improvement (EI) criterion, which estimates how much improvement can be achieved at each candidate point by considering both the predicted mean and uncertainty from the GP model. By maximizing EI, the algorithm selects sampling points that have a high probability of improving the objective, while avoiding unnecessary evaluations in less promising areas. The interested reader may refer to [44] for the details.

The climbing procedure, summarized in Alg. 1, for each position hole and its relative leg, the Motion Leg tries to position its Σ_{tool} at $\Sigma_{\text{target}} = (x_d, y_d, z_d)$. During the insertion phase the system continuously monitors the motor force signal f_{motor}. If the force exceeds a predefined threshold the insertion is halted. At this point, a cost value J_{BO} is computed to evaluate

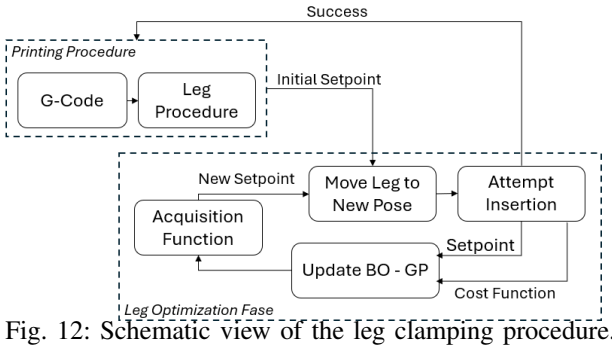

Fig. 12: Schematic view of the leg clamping procedure.

the attempted pose and BO algorithm is updated accordingly. A new candidate position is then selected by the AF, which balances exploration of uncertain regions with exploitation of promising areas. This iterative process continues until a successful insertion is achieved. Once convergence is reached, the learned model is retained and reused across successive WAAM layers, enabling faster convergence.

The cost function guiding the BO process is defined as:

$$J_{\text{BO}} = -\left(G_x e_x + G_{yz} e_{yz} + G_f e_f\right) \tag{10}$$

where $e_x = x_d - x$ is the axial insertion error along the x-axis, and $e_{yz} = \sqrt{(y_d - y)^2 + (z_d - z)^2}$ represents the radial misalignment in the yz plane. The interaction force error $e_f = f - f_d$ (if $f > f_d$, else $e_f = 0$) penalizes excessive insertion forces estimated via stepper motor current readings. If the force exceeds a critical threshold, the insertion is considered a failure, the optimization is halted, and a penalty is applied in the cost. Scalar weights G_x, G_{yz}, and G_f determine the relative importance of accurate positioning, radial alignment, and force compliance.

VII. Results

Experiments focus on climbing and anchoring, which are the main contributions of this work. Continuous WAAM deposition is outside the scope of this paper because it primarily concerns print-quality and material characterization, which are orthogonal to the proposed climbing/anchoring strategy. For completeness, we still report representative deposition trials to demonstrate that the integrated system can deposit and form WAAM beads. Climb a two level model is sufficient to validate the approach, since the same climbing and anchoring procedure repeats identically for additional levels.

A. Climbing Procedure

Fig. 13 illustrates the two-level climbing sequence (without BO). Figs. 13a–13d show the first level climb: the Vertical Actuator actuator raises the leg until the Anti-Pullout System shaft aligns with the WAAM-produced element; then the Horizontal Actuator actuator inserts the Anti-Pullout System into the Anchor Points on the structure wall. Next, the Clamping Device is actuated to lock the robot to the structure, providing the attachment for subsequent operations. The same sequence is executed sequentially for all four Motion Legs until the robot is fully anchored. Figs. 13e and 13f report the second level climb, which follows the same procedure with the additional

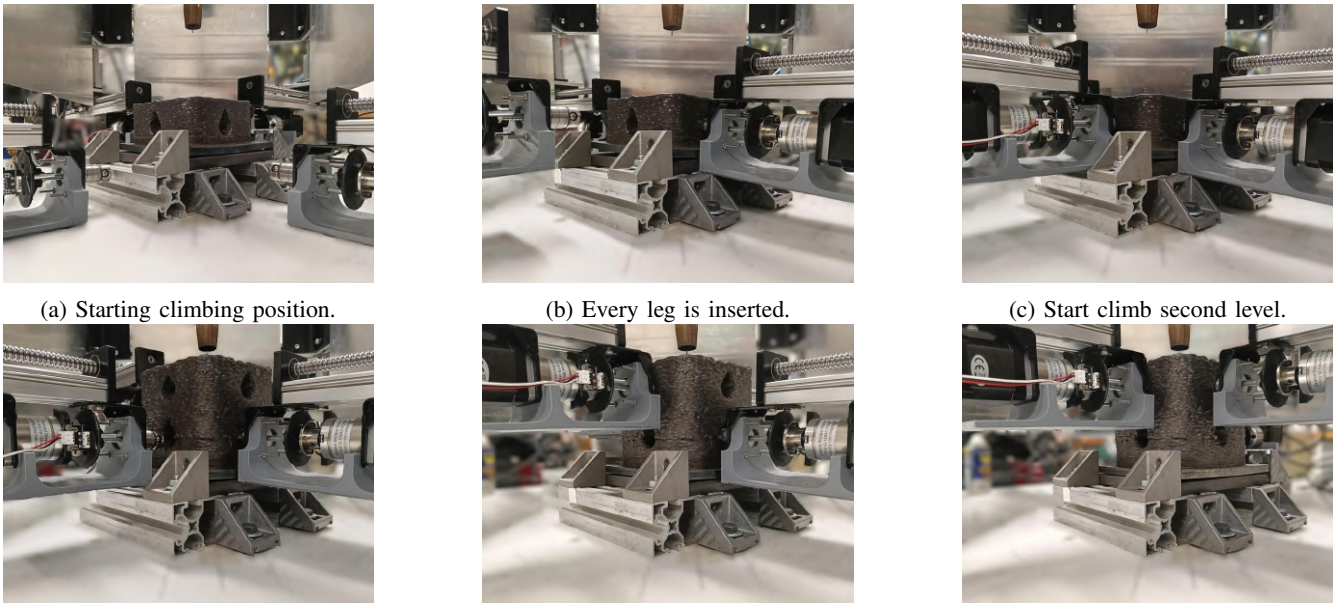

(a) Starting climbing position. (b) Every leg is inserted. (c) Start climb second level.

(d) Disarm leg from first level and insert in the second. (e) First leg climbs attaches to second level (f) Legs have reached the second level.

Fig. 13: CM3DP climbing sequence: a complete transition from the first to the second level.

step of disengaging the leg from the previous Anchor Points before re-alignment and insertion.

Because of geometric irregularities and misalignment of the holes (Tabs. I and II) the climbing procedure method can lead to two main issues: collisions during insertion, preventing the Clamping Device from engaging; and oversized holes, which may hinder proper locking and induce a slight tilt of the printer, potentially degrading the accuracy of subsequent insertions. To improve reliability, the insertion phase employs a feedback-based controller integrated with BO.

Fig. 14 reports an example of the BO procedure (Alg. 1) applied to the horizontal actuator of Leg 1; results generalize to the other legs via coordinate transformations. Overload detection is based on the motor current, using a 150 mA threshold: successful insertions keep the current below this value, while overloads are penalized to steer the optimizer away. The search space is defined around the nominal pose, and candidates far from the desired insertion point receive lower reward, guiding the optimizer back to feasible regions. For each symmetric leg pair, if the insertion at the nominal hole fails. In our tests up to 25 trials are allowed for the first leg and up to 10 for the second (due to kinematic constraints after the first insertion). The search space is discretized within $\pm 20\,\mathrm{mm}$ around the nominal pose, with a discretization step of $2\,\mathrm{mm}$. When the first insertion fails and the procedure is activated, the total insertion time is about 6 minutes per leg pair, dropping to 2 minutes when reusing the optimized model at subsequent levels. Convergence time mainly depends on the optimization bounds and discretization; tighter bounds and coarser steps can reduce the number of evaluated configurations when hole accuracy is higher.

As shown in Tab. V, the BO-based strategy achieves a failure rate below 10%. Failures can also occur when the search space is too restrictive or when the feedback-driven search does not locate a feasible hole configuration within the predefined number of trials. Overall, these results indicate that the proposed feedback approach is effective, and they also provide practical guidelines for improving success rate primarily by enlarging the search bounds and/or increasing the allowed number of exploration attempts.

B. WAAM deposition

This section evaluates whether the integrated CM3DP system can reliably deposit WAAM beads, focusing on printer functionality rather than process optimization. Experiments were conducted on the CM3DP using a Selco GSM-352 welding power source, 1.2 mm ER70S-6 steel wire, and an 82% Ar / 18% CO_2 shielding gas mixture at 15 L/min. Fig. 15 reports preliminary trials aimed at identifying feasible parameters both at the power-source level and on the CM3DP side. The welding current was varied from 75 A to 150 A. A representative setting at 130 A, with a printer TCP speed of 1000 mm/min and wire feed speed of 3.8 mm/min, provided a suitable quality thickness tradeoff. Under these conditions, the deposited bead exhibited approximately 3 mm width and a quasi uniform 1.5 mm height.
The selected parameters were then used to print a multi-layer square path representative of the baseline WAAM geometry, evaluating dimensional uniformity over three deposited layers. The G-code was generated from the CAD model by requesting

TABLE V: Comparison of plug insertion performance with and without Bayesian Optimization.

Method (Leg Pair)	N of Trials	Mean Time	Success Rate
Without BO	10	25 s	30%
With BO first level	10	6 min	90%
With BO next levels	10	2 min	92.5%

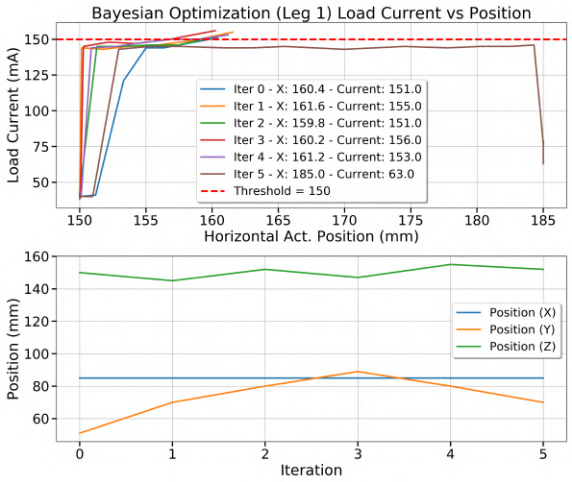

(a) Current vs. position of the horizontal actuator (top) and position setpoint from Bayesian Optimization (bottom). The insertion trajectory is interrupted if the current exceeds the threshold.

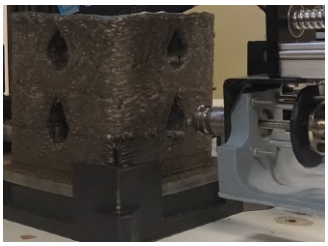

(b) Initial position.

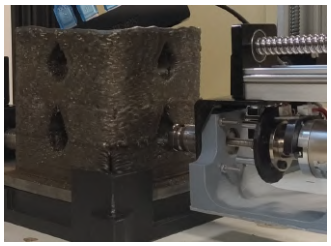

(c) First iteration failed because the wall was hit.

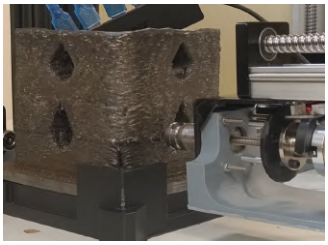

(d) Second iteration failed because the wall was hit.

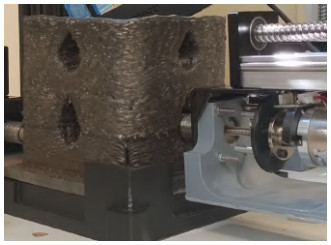

(e) Fifth iteration succeeded.

Fig. 14: Different phases of the insertion procedure guided by Bayesian Optimization.

a nominal toolpath speed of 1000 mm/min in the slicer. After the first layer, measurements along straight segments were consistent with the single-bead test (approximately 3 mm width and 1.4 mm height). However, at the rounded corners the deposition became non-uniform, reaching a maximum local height of 1.8 mm. As three additional layers were printed, corner over-deposition accumulated: the straight segments remained close to the expected value, while the corner region reached approximately 5.5 mm total height and not uniform. By manually adjusting the tool speed at the corner regions, the corner error was reduced and deposition quality augmented. These results validate the basic printing functionality of the integrated system, while indicating the need for dedicated G-code validation and corner-aware speed scheduling in future developments.

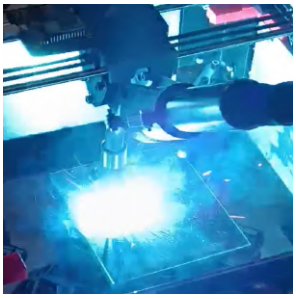

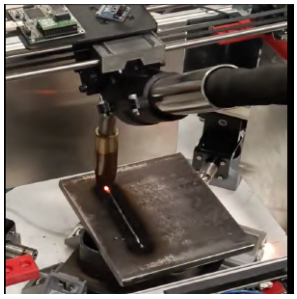

Print a single bead

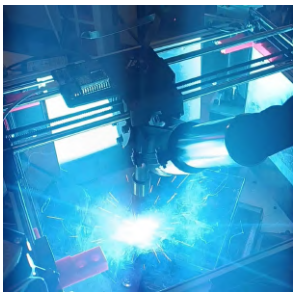

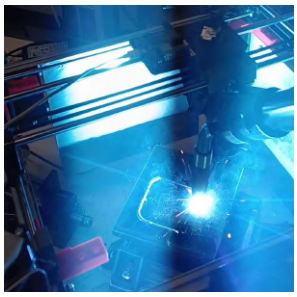

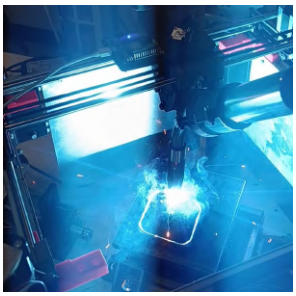

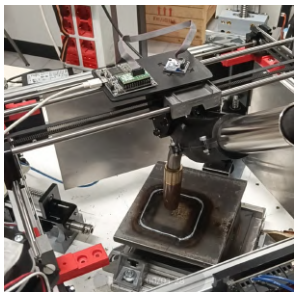

Print a three-layer squared tubular element

Fig. 15: Testing WAAM deposition using CM3DP

C. Frame Balancing

Residual Robot Frame tilt can degrade contact conditions and reduce stability during climbing, potentially increasing the load on one leg relative to the others. Therefore, the tilt is reduced via an IMU-based self-balancing routine (Sec. V-C) to limit inclination with respect to the gravity direction and mitigate issues during climbing.

Figure 16b illustrates the a case scenario where the hole diameter on one leg is larger than expected, causing the Robot Frame to tilt under its weight. In these cases, to proceed with climbing sequence the printer is re-leveled. As shown in Fig. 16c, the residual Robot Frame tilt is corrected and realigned with the horizontal printing plane . Fig. 16a shows the IMU angle measured (raw and low-pass filtered) during a balancing routine. A 0° reference is used as target in order to allign the Robot Frame with the plane; by adjusting the leg positions, the system reduces the orientation error and restores a stable posture.

VIII. Conclusion

This paper presented the design, working principle, and experimental validation of the CM3DP. The results, supported by a Bayesian Optimization approach, demonstrate the system's ability to handle the uncertainties inherent to WAAM

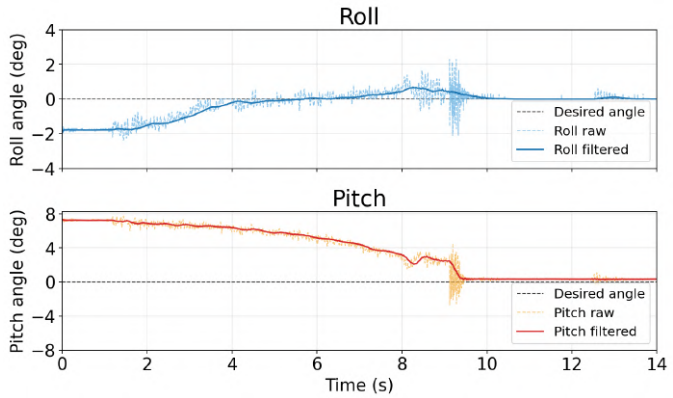

(a) IMU angle signal and filtered estimate, showing the tilt correction over time.

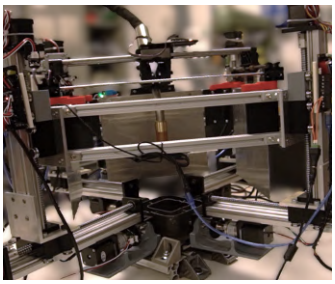

(b) Initial misalignment.

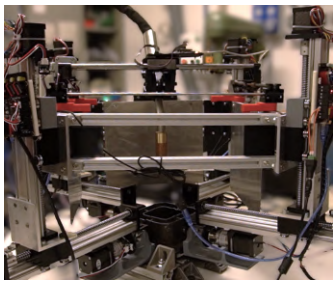

(c) Aligned configuration.

Fig. 16: Frame balancing during the first anchoring phase.

Technology. Despite the irregularities of the printed structures, the CM3DP successfully climbs the WAAM-produced element and maintains precise and stable operation, confirming the robustness of the proposed solution. In addition, the feasibility of the CM3DP to deposit WAAM steel material layers has been demonstrated through preliminary deposition tests, validating the capability of the integrated system to perform controlled metal deposition.

Some limitations related to the inherent geometrical imperfections of WAAM, such as burrs and bubbles affecting Anchor Points alignment, were successfully addressed. By integrating motor current feedback, the system is able to detect overloads during insertion attempts, preventing mechanical damage and enabling corrective strategies when a Clamping Device insertion fails.

Future work will focus on the coupled climbing–deposition operation through long-duration printing campaigns, together with a dedicated assessment of print quality and structural performance of WAAM-produced elements fabricated using the CM3DP system. Further developments of the CM3DP will aim at expanding the achievable geometric freedom within the working area and at advancing the WAAM deposition capabilities of the system. Within a longer-term perspective, successive evolutions of the CM3DP system may extend this geometric freedom toward more articulated structures, potentially including configurations such as tree-like structures (Fig. 17). Moreover, forthcoming work will present the experimental validation of WAAM material deposition while the CM3DP operates in climbing mode.

Fig. 17: Potential Application.

References

[1] G. Rasiya, A. Shukla, and K. Saran, "Additive manufacturing-a review," *Materials Today: Proceedings*, vol. 47, pp. 6896–6901, 2021, international Conference on Advances in Design, Materials and Manufacturing.

[2] J. J. Lewandowski and M. Seifi, "Metal additive manufacturing: A review of mechanical properties," *Annual Review of Materials Research*, vol. 46, no. 1, pp. 151–186, 2016.

[3] F. Martina, J. Ding, S. Williams, A. Caballero, G. Pardal, and L. Quintino, "Tandem metal inert gas process for high productivity wire arc additive manufacturing in stainless steel," *Additive Manufacturing*, vol. 25, pp. 545–550, 2019.

[4] M. Srivastava, S. Rathee, A. Tiwari, and M. Dongre, "Wire arc additive manufacturing of metals: A review on processes, materials and their behaviour," *Materials Chemistry and Physics*, vol. 294, p. 126988, 2023.

[5] L. Gardner, "Metal additive manufacturing in structural engineering–review, advances, opportunities and outlook," in *Structures*, vol. 47. Elsevier, 2023, pp. 2178–2193.

[6] X. Meng and L. Gardner, "Hybrid construction featuring wire arc additive manufacturing: review, concepts, challenges and opportunities," *Engineering Structures*, vol. 326, p. 119337, 2025.

[7] V. Laghi, L. Arrè, L. Tonelli, G. Di Egidio, L. Ceschini, I. Monzón, A. Laguía, J. A. Dieste, and M. Palermo, "Mechanical and microstructural features of wire-and-arc additively manufactured carbon steel thick plates," *The International Journal of Advanced Manufacturing Technology*, vol. 127, pp. 1391–1405, 2023.

[8] H. Kloft, L. P. Schmitz, C. Müller, V. Laghi, N. Babovic, and A. Baghdadi, "Experimental application of robotic wire-and-arc additive manufacturing technique for strengthening the i-beam profiles," *Buildings*, vol. 13, no. 2, 2023.

[9] L. Arrè, V. Laghi, A. M. Paola, and M. Palermo, "Tubular sandwich cross-sections fabricated with wire arc additive manufacturing for jumbo structural members," in *Structures*, vol. 67. Elsevier, 2024, p. 106689.

[10] V. Laghi, M. Palermo, L. Tonelli, G. Gasparini, V. A. Girelli, L. Ceschini, and T. Trombetti, "Mechanical response of dot-by-dot wire-and-arc additively manufactured 304l stainless steel bars under tensile loading," *Construction and Building Materials*, vol. 318, p. 125925, 2022.

[11] V.-A. Silvestru, I. Ariza, and A. Taras, "Structural behaviour of point-by-point wire arc additively manufactured steel bars under compressive loading," *Journal of Constructional Steel Research*, vol. 207, p. 107982, 2023.

[12] A. Spinasa, B. Weber, X. Meng, R. Zhang, M. Nitawaki, and L. Gardner, "Influence of process parameters on the physical and material properties of waam steels," *Construction and Building Materials*, vol. 479, p. 141078, 2025.

[13] N. Hadjipantelis, B. Weber, C. Buchanan, and L. Gardner, "Description of anisotropic material response of wire and arc additively manufactured thin-walled stainless steel elements," *Thin-Walled Structures*, vol. 171, p. 108634, 2022.

[14] M.-T. Chen, T. Zhang, Z. Gong, W. Zuo, Z. Wang, L. Zong, O. Zhao, and L. Hu, "Mechanical properties and microstructure characteristics of wire arc additively manufactured high-strength steels," *Engineering Structures*, vol. 300, p. 117092, 2024.

[15] B. Weber, X. Meng, R. Zhang, M. Nitawaki, T. Sagawa, and L. Gardner, "Tensile behaviour of waam high strength steel material and members," *Materials & Design*, vol. 237, p. 112517, 2024.

[16] L. Gardner, P. Kyvelou, G. Herbert, and C. Buchanan, "Testing and initial verification of the world's first metal 3d printed bridge," *Journal of constructional steel research*, vol. 172, p. 106233, 2020.

[17] B. Weber, X. Meng, and L. Gardner, "Optimised and 3d printed steel garden bridge: from design to experimental verification," *Automation in Construction*, vol. 181, p. 106638, 2026.
[18] T. Feucht, B. Waldschmitt, J. Lange, and M. Erven, "Additive manufacturing of a bridge in situ," *Steel Construction*, vol. 15, no. 2, pp. 100–110, 2022.
[19] M. Mavros, N. Hadjipantelis, I. Ioannou, O. Kontovourkis, and A. Georgiou, "In-plane strengthening of heritage masonry structures using 3d-printed steel reinforcement: Experimental proof-of-concept," *Construction and Building Materials*, vol. 499, p. 143746, 2025.
[20] H. A. Jassmi, F. A. Najjar, and A.-H. I. Mourad, "Large-scale 3d printing: The way forward," *IOP Conference Series: Materials Science and Engineering*, vol. 324, no. 1, p. 012088, mar 2018.
[21] A. Puzatova, P. Shakor, V. Laghi, and M. Dmitrieva, "Large-scale 3d printing for construction application by means of robotic arm and gantry 3d printer: A review," *Buildings*, vol. 12, no. 11, 2022.
[22] Z. Zuo, W. D. Corte, Y. Huang, X. Chen, Y. Zhang, J. Li, L. Zhang, J. Xiao, Y. Yuan, K. Zhang, L. Zhang, and V. Mechtcherine, "Strategies towards large-scale 3d printing without size constraints," *Virtual and Physical Prototyping*, vol. 19, no. 1, p. e2346821, 2024.
[23] J. Ulrich Weber, M. Buhr, B. Vykhtar, A. Fischer, K. Gritz, and P. Schlüter, "Mobile refurbishment by robot-based additive manufacturing," in *2022 IEEE 5th International Conference on Industrial Cyber-Physical Systems (ICPS)*, May 2022, pp. 1–6.
[24] M. Palermo, T. Trombetti, and V. Laghi, "Stampante tridimensionale, relativo procedimento per la realizzazione di un oggetto stampato ed oggetto così ottenuto," Patent IT102 020 000 024 109, 2022.
[25] T. Tabassum and A. Ahmad Mir, "A review of 3d printing technology-the future of sustainable construction," *Materials Today: Proceedings*, vol. 93, pp. 408–414, 2023, uKIERI Concrete Congress – 'Sustainable Concrete Infrastructure'.
[26] WASP, "Wasp 3d printers [website]."
[27] K. Navaneetha, M. S. Kumar, A. V. S. Reddy, P. S. S. Babu, and K. Jagan Mohan Reddy, "Modeling of two link manipulator used for 3d printing," *IOP Conference Series: Materials Science and Engineering*, vol. 1057, no. 1, p. 012023, 2021.
[28] B. 3D, "Blackbelt 3d [website]."
[29] O. Lakhal, T. Chettibi, A. Belarouci, G. Dherbomez, and R. Merzouki, "Robotized additive manufacturing of funicular architectural geometries based on building materials," *IEEE/ASME Transactions on Mechatronics*, vol. 25, no. 5, pp. 2387–2397, 2020.
[30] C. Balaguer, A. Giménez, J. Pastor, V. Padrón, and M. Abderrahim, "A climbing autonomous robot for inspection applications in 3d complex environments," *Robotica*, vol. 18, no. 3, pp. 379–388, 2000.
[31] C. Balaguer, A. Giménez, and A. Jardon Huete, "Climbing robots' mobility for inspection and maintenance of 3d complex environments," *Autonomous Robots*, vol. 18, no. 3, pp. 157–172, 2005.
[32] T. A. M. Salet, Z. Y. Ahmed, F. P. Bos, and H. L. M. Laagland, "Design of a 3d printed concrete bridge by testing," *Virtual and Physical Prototyping*, vol. 13, no. 6, pp. 734–743, 2018.
[33] B. Jenett and D. Cellucci, "A mobile robot for locomotion through a 3d periodic lattice environment," *2017 IEEE International Conference on Robotics and Automation (ICRA)*, pp. 5474–5479, 2017.
[34] B. Hoshnevis, "Automated construction of towers and columns," Patent CN 106 536 142 B.
[35] Y. Liu, H. Kim, and T. Seo, "Anyclimb: A new wall-climbing robotic platform for various curvatures," *IEEE/ASME Transactions on Mechatronics*, vol. 21, no. 4, pp. 1812–1821, 2016.
[36] Y. Guan, H. Zhu, W. Wu, X. Zhou, L. Jiang, C. Cai, L. Zhang, and H. Zhang, "A modular biped wall-climbing robot with high mobility and manipulating function," *IEEE/ASME Transactions on Mechatronics*, vol. 18, no. 6, pp. 1787–1798, 2013.
[37] A. Kemmer, M. Snyder, and M. Chen, "Extended structures of additive manufacturing," Patent US 2015/0 076 732 A1, March, 2015, publication Date: March 19, 2015.
[38] M. Wang and R. Li, "A self-elevating 3d printing device and method for construction," patent CN 104 149 345 A.
[39] H.-A. Lee and H.-H. Lee, "Multi-joint wall-climbing robot using vacuum pads," patent KR 20 170 121 768 A.
[40] H. Keller, P. Kuhn, and D. Meiners, "Method of constructing a tower," 2017, uS Patent 2017/0016244 A1.
[41] K. Kanzler, "Kletterdruckeinrichtung sowie verfahren zum 3d-drucken eines werkstücks," Patent EP 3 072 670 A1, 2015.
[42] X. S. Gao, D. Q. Cui, D. S. Chen, Y. Lei, F. L. Qi, H. Dong, and L. J. Zhang, "Dual-sided liquid cooling for 3d stacked chip heat dissipation," patent CN 105 235 764 B.
[43] S. Lahteine, E. van der Zalm, R. Neufeld, K. Bennet, and et all, "Marlin," 2021.
[44] P. I. Frazier, "A tutorial on bayesian optimization," 2018. [Online]. Available: https://arxiv.org/abs/1807.02811

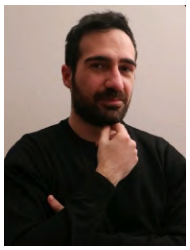

Andrea Govoni received his M.Sc. degree in Automation Engineering from the University of Bologna, Italy, in 2020. He is currently pursuing a Ph.D. in the Department of DEI at the University of Bologna. His research interests focus on the model and data driven control of industrial robotic manipulators.

Lidiana Arrè is currently pursuing a Ph.D. in Structural Design at the University of Bologna. Her research focuses on the cutting-edge field of metal Wire Arc Additive Manufacturing (WAAM) for applications in the Architectural, Engineering and Construction (AEC) sector. Her research interests include innovation in AEC, Design for Additive Manufacturing (DfAM) and Life Cycle Assessment (LCA).

Robin Joseph received an M.Sc. degree in Automation Engineering from the University of Bologna. He is currently working as a software developer in an automation company. His research interests include robotics and automation, with a particular focus on control systems, robotic manipulation, and intelligent automation technologies.

Davide Samorì received his M.Sc. degree in Electronic Engineering from the University of Bologna, Italy. He is currently a laboratory technician and adjunct professor in the Department of DEI at the University of Bologna. His current research interests include PCB Design, microprocessor system, electric drives and motor control.

Alessando Ascari is an assistant professor at the Department of Industrial Engineering, University of Bologna and he got his Ph.D in laser joining of advanced, cellular and hybrid materials. He has been involved in studying laser-based processes for more than 15 years with particular attention to surface hardening, advanced welding and direct metal deposition.

Michele Palermo is Associate Professor at the Department of Civil and Environmental Engineering at the University of Bologna, Italy. His research focuses on seismic engineering, automation, and metal additive manufacturing (AM) in construction. He is a member of the European TG8 task group, ASTM Committee F42 on AM, and the COST Action Circular B, with emphasis on AM sustainability in construction. He leads the Automation and Additive Manufacturing in Construction research group at the University of Bologna. He holds three AM-related patents and is involved in several national and European metal AM projects.

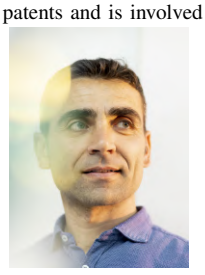

Gianluca Palli is currently Full Professor at the University of Bologna. His research interests include robots for unstructured environments, deformable objects manipulation and human-robot cooperation. He is the author or co-author of more than 160 scientific papers in international journals and conferences. He coordinated the REMODEL H2020 project, aiming at the development of robotic technologies for complex deformable linear object manipulation, and is now the coordinator of the HE IntelliMan project, aiming at the development of AI-based manipulation systems for robotic services, industrial manufacturing, and prosthetics.

Response to Reviewers

Mechatronic Development of a Climbing Robot for Continuous WAAM 3D Printing
IEEE/ASME Transactions on Mechatronics – Paper ID: *TMECH-07-2025-21529*

We thank the Editor and the Reviewers for their constructive feedback. Below we address each comment point-by-point. Changes in the revised manuscript are indicated in red in the submitted article and we refer to the updated sections/figures/tables where appropriate.

Modifications

- To address the reviewers' requests, we integrated the new torch module, enabling the framework to perform WAAM printing. To accommodate the added technical description and the new discussion introduced in this revision. The text was condensed without removing essential content or altering the technical contribution.
- For clarity, all revised or newly added text is highlighted in red, including edits made for consistency and integration purposes (not only those directly requested by the reviewers). We will not highlight the text if it is modified only for summarization.
- Authorship update: Compared to the previous submission, we added two authors who contributed to the integration of the WAAM torch/end-effector and related experimental setup. The author list and contributions have been updated accordingly

Technical Editor

1. **Comment:** Two reviewers have reviewed the paper. Another reviewer has agreed but despite different reminder the report was not submitted. To compensate for this, an additional reviewer might be invited in the next round. Nethertheless, the other two reviewers have provided a quite detailed and consistent assessment which shows the interest of the topic, but at the same time the fact that the manuscript needs serious revision before being accepted. Because the comments seem reasonable and carefully put, all of them should be carefully addressed in a revised version of the manuscript.

Response:
We thanks the technical editor for the comment and for the thorough assessment of the manuscript. We appreciate the effort invested by the two reviewers, and we understand that an additional reviewer may be invited in the next round to complete the evaluation. In the revised version, we have implemented substantial changes to address all comments in depth, including major restructuring and clarifications, as well as additional validation and improved presentation. We believe these revisions significantly strengthen the manuscript and provide a more solid and mature contribution to the field.

Reviewer #1

1. **Comment:** It would be useful to add some information about the ultimate performance of the printed structures and how that might be affected by this method of construction e.g. will the structural behaviour be as good as normal, or better. Several studies on the structural behaviour of WAAM elements have been conducted. Also, can the method be applied in the area of hybrid construction, when WAAM material is deposited onto traditional steelwork. There are numerous papers on the structural performance of WAAM elements and hybrid elements that would be of interest. e.g. those by Dr Xin Meng and Dr Ben Weber.

Response:
The authors thank the Reviewer for this valuable comment. In response, the manuscript has been revised to integrate additional information on existing studies concerning the material behaviour of WAAM-produced elements. The section dedicated to the state of the art of WAAM has been expanded accordingly, in order to better clarify the current level of knowledge on WAAM materials and to highlight their relevance and potential for applications in the construction field.
Regarding the applicability of the CM3DP system within hybrid construction scenarios, the authors note that this possibility can be considered by adopting appropriate design measures that satisfy the operational requirements of the CM3DP, including the use of discrete guiding and anchoring mechanisms. However, the investigation of hybrid construction applications is not the focus of the present work and is therefore left outside the scope of this study.
Accordingly, additional references related to the aspects outlined above have been included in the revised manuscript.
We added the references at the end of the letter: [1–11]

Reviewer #2

1. **Comment:** The authors claim that “The proposed CM3DP system is designed to fabricate self-supporting structures with predominantly longitudinal development and potentially infinite length, such as the tree-like structures shown in Fig. 2(a).” This assertion is misleading. In practice, the system only demonstrates self-supportability for drop-shaped holes. For truss-like or branching structures, members inclined beyond the overhang threshold cannot be realized, since overhang formation is governed solely by the angle between gravity and the structural inclination, which is not alleviated by repositioning the printer. Consequently, the tree-like structure shown in Fig. 2(a) cannot realistically be fabricated using the proposed approach.

Response:
The authors thank the Reviewer for this comment and acknowledge that the original formulation could be interpreted as misleading. In response, the manuscript has been revised to clarify the scope and limitations of the proposed CM3DP system and to avoid any ambiguity regarding the fabrication of branching or tree-like structures. Specifically, the reference to tree-like configurations has been removed from Section 3, which now strictly describes the capabilities demonstrated by the current CM3DP system. In this section, the CM3DP is explicitly presented as a system designed to fabricate self-supporting elements characterized by predominantly longitudinal development, rather than complete branching or tree-like structures. The reference to tree-like configurations has been retained only in the Conclusions, where it is clearly framed as a long-term research perspective. In this context, such configurations are discussed as potential outcomes of future developments and successive evolutions of the CM3DP system, rather than as geometries directly fabricated using the present approach. The current system is therefore limited to the fabrication of individual components compatible with WAAM process constraints, while future advancements in system design and process control may extend its applicability toward more complex structures.

2. **Comment:** Although the system is presented as a mobile 3D printer, the experimental results focus exclusively on the climbing function. No details of the WAAM process or nozzle integration are provided. As such, the work essentially demonstrates a climbing robot, not a complete 3D printing system. This substantially narrows the contribution relative to the claims made.

Response:
We thank the reviewer for the insightful comment. While the experimental campaign in the previous version emphasized the climbing capability, our intent was not to re-investigate WAAM itself, which is a well-established and widely industrialized process. The main contribution of this work lies in a design of the overall system-level and climbing tests. Nevertheless, we agree that the previous manuscript lacked experimental evidence of the printing functionality. For this reason, we have revised the robot frame to properly accommodate the nozzle integration and we added a dedicated Results VII.B subsection reporting printing trials and representative printed samples. As a result, the manuscript now explicitly demonstrates both the climbing and the WAAM printing capabilities of the proposed system.

3. **Comment:** The calibration method introduced in Section V-B is potentially the most valuable contribution. However, the equations are designed only to realign the system with the horizontal plane, confining printability to strictly vertical columns. To extend the utility of this contribution, the calibration framework should be generalized to handle inclined planes and non-vertical configurations.

Response:
We thank the reviewer for highlighting the potential impact of the calibration routine in Sec. V-B. In the current manuscript, we intentionally validate the self-balancing/calibration method only for vertical structures, consistently with the problem setting and assumptions stated in Sec. III. The aim of Sec. V-B is to reduce the residual tilt after anchoring and to improve alignment during climbing and subsequent insertions on vertical elements; it is not meant to provide a general calibration or planning framework for arbitrary surface orientations.
Generalizing the approach to inclined planes and non-vertical configurations is an interesting direction, but it would require (i) additional modeling and redesign to accommodate contact/anchoring on slanted surfaces; in the current hardware, the admissible inclination is limited to approximately 6° before mechanical interferences, and (ii) substantially broader experimental validation across multiple surface orientations and defect conditions on printing elements. Indeed climbing along inclined structures would also imply tilting the printing plane, which introduces additional process-related challenges for WAAM (e.g., gravitational effects on molten pool stability and bead geometry) that are outside the scope of this work. For these reasons, we consider the proposed generalization beyond the scope of the present manuscript, whose primary contribution is robust climbing and anchoring on vertical WAAM structures.

4. **Comment:** The authors justify their focus on climbing alone by arguing that WAAM printing is time-consuming. However, the climbing system itself is not inherently tied to WAAM. A straightforward alternative would be to test the device using a simpler FDM nozzle, thereby enabling demonstration of a combined print-and-climb process. This would provide a much stronger validation of the concept.

Response:
We appreciate the Reviewer's suggestion. However, the proposed CM3DP system has been specifically developed to enable climbing-based additive fabrication using a WAAM torch, and its design explicitly accounts for constraints that are intrinsic to WAAM deposition. These include, among others, the geometry and size of the welding torch, its weight, the associated cabling, and the interaction with WAAM-induced geometric irregularities. As a consequence, validating the system using a deposition process such as FDM would not provide a meaningful assessment of the proposed approach. An FDM nozzle operates under substantially different integration conditions. Testing the climbing system with such a process would therefore bypass the critical challenges that the CM3DP has been designed to address and would not constitute a fair or representative validation of the system. For this reason, the validation strategy deliberately targets the intended WAAM setting. The deposition of single WAAM beads and of a squared tubular element demonstrates a first, necessary step toward the combined climb-and-print concept, namely the feasibility of depositing WAAM material layers using the integrated system. Alternative demonstrations of climbing-based deposition with simpler processes are already available in the literature [12].

Sincerely,
Andrea Govoni

References

[1] L. Gardner, "Metal additive manufacturing in structural engineering–review, advances, opportunities and outlook," in *Structures*, vol. 47. Elsevier, 2023, pp. 2178–2193.

[2] X. Meng and L. Gardner, "Hybrid construction featuring wire arc additive manufacturing: review, concepts, challenges and opportunities," *Engineering Structures*, vol. 326, p. 119337, 2025.

[3] L. Arrè, V. Laghi, A. M. Paola, and M. Palermo, "Tubular sandwich cross-sections fabricated with wire arc additive manufacturing for jumbo structural members," in *Structures*, vol. 67. Elsevier, 2024, p. 106689.

[4] A. Spinasa, B. Weber, X. Meng, R. Zhang, M. Nitawaki, and L. Gardner, "Influence of process parameters on the physical and material properties of waam steels," *Construction and Building Materials*, vol. 479, p. 141078, 2025.

[5] N. Hadjipantelis, B. Weber, C. Buchanan, and L. Gardner, "Description of anisotropic material response of wire and arc additively manufactured thin-walled stainless steel elements," *Thin-Walled Structures*, vol. 171, p. 108634, 2022.

[6] M.-T. Chen, T. Zhang, Z. Gong, W. Zuo, Z. Wang, L. Zong, O. Zhao, and L. Hu, "Mechanical properties and microstructure characteristics of wire arc additively manufactured high-strength steels," *Engineering Structures*, vol. 300, p. 117092, 2024.

[7] B. Weber, X. Meng, R. Zhang, M. Nitawaki, T. Sagawa, and L. Gardner, "Tensile behaviour of waam high strength steel material and members," *Materials & Design*, vol. 237, p. 112517, 2024.

[8] L. Gardner, P. Kyvelou, G. Herbert, and C. Buchanan, "Testing and initial verification of the world's first metal 3d printed bridge," *Journal of constructional steel research*, vol. 172, p. 106233, 2020.

[9] B. Weber, X. Meng, and L. Gardner, "Optimised and 3d printed steel garden bridge: from design to experimental verification," *Automation in Construction*, vol. 181, p. 106638, 2026.

[10] T. Feucht, B. Waldschmitt, J. Lange, and M. Erven, "Additive manufacturing of a bridge in situ," *Steel Construction*, vol. 15, no. 2, pp. 100–110, 2022.

[11] M. Mavros, N. Hadjipantelis, I. Ioannou, O. Kontovourkis, and A. Georgiou, "In-plane strengthening of heritage masonry structures using 3d-printed steel reinforcement: Experimental proof-of-concept," *Construction and Building Materials*, vol. 499, p. 143746, 2025.

[12] M. Palermo, T. Trombetti, and V. Laghi, "Stampante tridimensionale, relativo procedimento per la realizzazione di un oggetto stampato ed oggetto così ottenuto," Patent IT102 020 000 024 109, 2022.